Self-Seeding Effect on Primary Nucleation of Isotactic Polystyrene

Al Mamun, Susumu Umemoto, and Norimasa Okui*

Department of Organic and Polymeric Materials, International Polymer Research Center, Tokyo Institute of Technology, O-okayama, Meguro-ku, Tokyo, Japan

Nobuhide Ishihara

Materials Research Laboratory, Idemitsu Co., Ltd., Anesaki-kaigan, Ichihara-shi, Chiba, Japan

Received April 26, 2007; Revised Manuscript Received June 13, 2007

ABSTRACT: Primary nucleation behavior of isotactic poly(styrene) was studied in a wide range of crystallization temperatures (T_c), times, and melt temperatures (T_f). Samples were melted at several melt temperatures (T_f) from 225 to 250 °C (or vice versa) and then isothermally crystallized. Time dependence on the nucleation behavior showed a sigmoidal curve with an induction time (τ_0). The spherulites sporadically appeared (the steady state of nucleation, I) until they reached a limiting number of nuclei (the saturated nucleation density, N_s). The number of nuclei reached saturation much earlier than the induction time (τ_{over}) in the overall crystallization. N_s was not associated with impingement of spherulites, since about 90% of the melt region remained. It was found that there was a critical spherulite size, in which induced nucleation sites began to appear within the outline of the original spherulite in the subsequent crystallization. When the crystallization was stopped before reaching the critical spherulite size, there was no melt temperature dependence on the nucleation behavior. On the other hand, when spherulites were grown beyond the critical spherulite size, a large number of small spherulites (granular structure) appeared within the outline of the original spherulite in the subsequent crystallization. The number of additional nucleation sites increased with an increase in the original spherulite size, and the increment of nucleation sites decreased with an increase in T_f. These granular structures could be due to insufficient melting of the crystal structure in the original spherulite, which will induce nucleation sites as a self-seeding effect upon subsequent crystallization. N_s increased by a factor of several thousand with a decrease in T_f from 250 to 225 °C. The crystallization temperature dependence on the nucleation rate has a bell-shaped curve with a maximum nucleation rate (I_{max} at T_{imax}). Both I_{max} and T_{imax} decreased with an increase in T_f up to about 240 °C and then remained constant values. I_{max} is a function of nucleation sites and is expressed by a power law of $N_s^{0.5}$. The nucleation density was found to be a function of the amount of 3_1-helix composed with 5 monomeric units remaining in the melt.

Introduction

Crystallization behaviors of polymeric materials are characterized by primary nucleation and crystal growth rates. There are two types of primary nucleation: homogeneous and heterogeneous nucleation. Homogeneous nucleation can be defined by spontaneous aggregation of polymer molecules to form a three-dimensional nucleus, which must be above a certain critical size below the melting point. Above this size, the nucleation occurs sporadically. In heterogeneous nucleation, nucleation sites preeexist in a sample and are activated instantaneously or sporadically with an induction time. These sites can be related to impurities in a bulk sample, a substrate surface, and some crystal fragments in the melt. When a polymer is melted at temperatures below (partial melting) or above (complete melting) the end of DSC melting curve, the number of nuclei changes drastically and strongly depends on the previous temperature of melting. Even above the melting point, if the melt temperature or its holding time is insufficient, remnants of the previous structure (residual crystal) can act as predetermined nucleation sites upon subsequent cooling.[1−10] Such a phenomenon is referred to as self-nucleation or memory effect. When a polymer is melted at a sufficiently high temperature for a long time, all memory of the previous crystalline structure can be removed. Such temperatures are usually higher than the equilibrium melting point.

* To whom correspondence should be addressed. E-mail: okui.n.aa@m.titech.ac.jp.

Self-seeding effects are often observed during crystallization of polymeric materials. There are two types of self-seeding effects. One is a crystal fragment after insufficient melting of a sample[1−10] constructing a molecular cluster or embryo in the melt. The other is related to an effect of flow fields, orienting, and deforming polymer molecules in the molten state.[11−15] Memory effects have been studied as a function of many experimental conditions, such as heating rate, melt temperature, holding time, and others. Such thermal histories in polymeric materials dominate the nucleation behavior. For example, the melt temperature plays an important role in determining overall crystallization rate. The overall crystallization rate increases with the rise in the residual nuclei or in the initial degree of crystallinity.[16] Various experimental conditions as noted above often produce nucleation data that are widely dispersed and not reproducible. However, reproducible results can be obtained when experimental conditions are controlled in a rigorous manner.[17]

Most previous works have studied overall crystallization measured by dilatometry, DSC, X-ray, IR, and many other methods. The overall crystallization rate is a function of linear crystal growth rate and primary nucleation rate. In order to clarify the nucleation mechanism details, direct observation of nucleation is required. In this present paper, we independently measured primary nucleation and crystal growth rate over a wide range of temperatures, times, and melt temperatures.

10.1021/ma070963j CCC: $37.00
Published on Web 07/27/2007

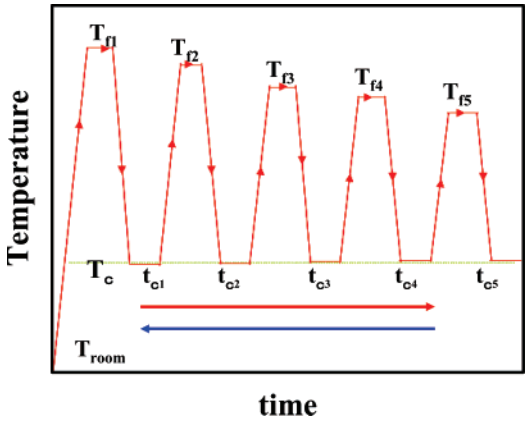

Figure 1. Schematic diagram of the thermal history used during isothermal crystallization at T_c for a period of time t_c from molten state of T_f under optical microscope. Isothermal crystallization was performed by repeatedly changing melt temperature (T_f) from higher to lower (or from lower to higher).

Experiments

Isotactic poly(styrene) (i-PS) (M_w = 17 800, M_n = 10 600, M_w/M_n = 1.68, tacticity: 96%) was supplied by Idemitsu Kosan Co., Ltd. The sample was melted between two cover glass plates with a 20 μm thick spacer on a hot stage. To erase any previous thermal history, the sample was initially melted at 250 °C, which is higher than the equilibrium melting point ($T_m°$ = 242 °C). The equilibrium melting temperature was determined by the Hoffman−Weeks extrapolation. DSC melting curve for i-PS crystallized at 200 °C for 8 h starts at about 210 °C and ends at 228 °C (tail of the curve).[17] In a typical experiment, the sample was melted for 5 min at several different melt (fusion) temperatures (T_f) between 225 and 250 °C. The thermal history of crystallization from the melt is schematically shown in Figure 1. For example, the sample was melted at T_{f1} (above $T_m°$) for 5 min, then cooled to a given crystallization temperature at T_c at a cooling rate of 30 °C/min, and subsequently crystallized at T_c for a certain period of time (t_c). After the crystallization time of t_c, the sample was heated at 30 °C/min to a melt temperature of T_{f2} that was below the previous temperature of melting (decreasing T_f) and held there for 5 min. The sample was then cooled to the same previous crystallization temperature of T_c and held there for a period time of t_c. This crystallization process was performed repeatedly, changing the melt temperature from higher to lower T_f (or from lower to higher T_f), as shown in Figure 1. Nucleation rate was measured on a Linkam LK-600FTIR temperature-controlled apparatus of under an Olympus BH-2 optical microscope (OM) equipped with a Pixel 600ES-CU CCD camera. The nucleation rate was estimated by counting the number of spherulites appearing sporadically as a function of time, and their numbers were normalized by the measured area under OM and the specimen's thickness. Linear crystal growth rate was measured by spherulite radius as a function of time. The crystal melting temperature was recorded on a Shimazu TA60 (DSC) at a heating rate of 5 °C/min. Infrared spectra of the samples were measured by a transmission method using a Jasco FT-IR 7000 Fourier transform IR system equipped with Metler HP-80 hot stage in a dry nitrogen atmosphere. For in-situ IR measurements, the sample was heated immediately after crystallization at 160 °C for 8 h. The spectra were recorded at 5 °C intervals at a heating rate of 2 °C/min from 160 to 260 °C.

Results and Discussion

Temperature Dependence of Primary Nucleation without Self-Seeding Effect. The sample was melted at 250 °C (T_{f1}) in order to erase the previous thermal history, and then it was cooled to 160 °C (T_c) under the crystallization process, as shown in Figure 1. Figure 2 shows the time dependence on the number of spherulites crystallized under the above conditions. The time

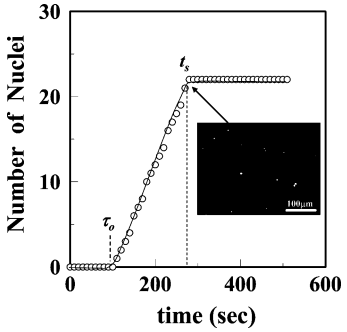

Figure 2. Time dependence on the number of nuclei crystallized at 160 °C from the melt at 250 °C. The arrow indicates where the melt region remains about 90%, and the optical micrograph image of small spherulites was taken. t_s denotes the time at which the number of nuclei is saturated, and τ_0 denotes the induction time.

dependence of the nucleation behavior starts with an induction time (τ_0), after which small spherulites appear sporadically. The number of the spherulites increases with time until it reaches a limiting number. The limiting number (saturated nucleation density, N_s) remained unchanged until the end of crystallization. Crystal nuclei are difficult to observe directly by common experimental methods because they are very small. Therefore, small spherulites are assumed to start at active individual sites, and they are only observed after a certain induction time, whereas the aggregation of polymer molecules is reversible up to a critical size. Beyond that time, a nucleus with a size greater than the critical size grows steadily, and the number of nuclei increases linearly with time. Therefore, nucleation rate was estimated by the number of nuclei per unit volume vs time. Here, the unit volume used was the initial volume under the optical microscope to determine a nominal nucleation rate. In practice, the volume of the noncrystalline domain decreases as crystallization proceeds, and the real nucleation rate must be adjusted for actual residual volume. The real nucleation rate, once corrected, coincided with the nominal nucleation rate within experimental error, since the residual region was large enough. However, the real nucleation rate will diverse from the nominal nucleation rate as the residual melt region becomes small. Therefore, only the nominal nucleation rate (I) is employed in this paper.

Induction time (τ_0) is the period of time to achieve critical nucleus formation and is often employed as the primary nucleation rate, since the nucleation rate is proportional to the inverse of the induction time.[17] The total number of nuclei is limited to a constant value (N_s) before the crystallization is completed. Saturated nucleation behavior has been found for many polymers.[1,5,7,17−21] It is interesting to note that the saturated density of N_s is proportional to the product of I and τ_0.[17] In fact, the product of $I\tau_0$ is a constant based on the nucleation theory reported by Frish.[22] However, the details in the saturation number have not been discussed yet. The residual melt region at the position indicated by the arrow in Figure 2 is still about 90%, and the time at this position is denoted as t_s. The limiting values are not associated with a reduction in the space available for nucleation, such as impingement among spherulites. In i-PS, the primary nucleation rate is much faster than the crystal growth rate, which results in many small spherulites.[17] In contrast, for poly(ethylene oxide) (PEO) the primary nucleation rate is much slower than the crystal growth rate, yielding fewer but larger spherulites.[1,2] Therefore, i-PS is an ideal polymer to study the primary nucleation mechanism.

When the sample was crystallized at 160 °C (T_c) for a certain period of time (t_c) from the melt at 250 °C (T_{f1}), the crystal-

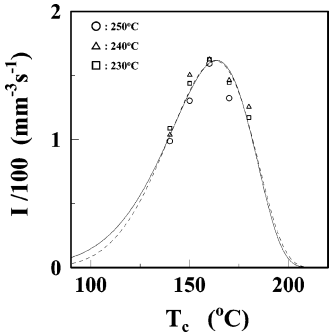

Figure 3. Temperature dependence on the nucleation rate for type A: partial crystallization with spherulite growth stopped below the critical size, from the melt at three different temperatures as indicated in the figure. Solid and broken lines represent curve fitting based on eq 1. Arrhenius (solid) and WLF (broken) expressions are used for the molecular transport term in eq 1.

lization was stopped immediately after the spherulites grew up to a few microns in size. Subsequently, the sample was melted at 230 °C (T_{f2}) for 5 min and then crystallized again at the same crystallization temperature (160 °C) according to the crystallization process shown in Figure 1. The sample crystallized after the above procedure is defined as type A: partial crystallization with spherulite growth stopped below a few microns in size. The same number of spherulites appeared at the same places. This result indicates that nuclei for the spherulites are influenced by the substrate surface. Here, the spherulites were not grown to a large size before t_s, as indicated in Figure 2, because of the slow crystal growth rate of i-PS. When the crystallization was stopped before the spherulites grew to a few microns in size from the molten state at T_f, the nucleation rate and the saturated nucleation density were not influenced by T_f above 225 °C. It has been reported that the duration time of melting is important for nucleation rate at higher temperature regions.[6−10] However, the nucleation behaviors in this study were independent of the melt time within the investigated range of times and temperatures. Figure 3 shows the temperature dependence of the nucleation rate in the case of type A from the molten state for three different melt temperatures. There is no melt temperature dependence, though a single, bell-shaped curve is observed. In addition, the temperature dependence of the linear crystal growth rate (G) of i-PS was not influenced by the melt temperature (T_f).

Sporadic nucleation rate is often expressed by the following equation proposed by Turnbull and Fisher.[23]

$$I = I_0 \exp[-\Delta E/RT - \Delta F/RT] \quad (1)$$

where I_0 is assumed to be a constant without temperature dependence but strongly depends on the number of nucleation sites and molecular weight.[24] ΔE is the activation energy for molecular transport process. ΔF is the work required to form a nucleus of critical size. The first term (ΔE) and the second term (ΔF) in eq 1 have opposite temperature dependencies, thereby bringing about a maximum in I_{max} at T_{imax}. Here, ΔF is commonly expressed as $\Delta F = KT_m^{o2}/\Delta T^2$, and K is expressed as $K = n\sigma_e\sigma_s^2/\Delta H_m^2$, where n is a mode of nucleation, ΔH_m is the heat of fusion, and σ_e and σ_s are the end- and lateral-surface free energies, respectively. ΔT is the degree of supercooling ($T_m^\circ - T$), where T_m° is the equilibrium melting temperature and T is crystallization temperature. R is a gas constant. The transport term can be expressed in terms of either an Arrhenius-type equation or a WLF-type equation.[17,24] Solid (Arrhenius-type) and broken (WLF-type) lines in Figure 3 are the results for curve fitting based on eq 1. It is clear that both expressions can sufficiently fit the data. In this report, discussions involving the molecular transport term use values derived from the Arrhenius curve fitting.

Temperature Dependence of Nucleation Rate with Self-Seeding Effect. Any memory from previous crystallizations were effectively removed at 250 °C (T_{f1}). The spherulite size was controlled as a function of crystallization time (t_{c1} at T_c), and then the crystallization was stopped. Figure 4 shows spherulites grown at that time (t_{c1}). Subsequently, the crystallized sample was melted at 230 °C (T_{f2}) for 5 min according to the crystallization process shown in Figure 1. Here, the size-controlled spherulite is called the original spherulite, and the sample crystallized under these conditions is defined as type B: partial crystallization as a function of spherulite size. When the sample is crystallized at 160 °C from the melt at 230 °C (T_{f2}), a large number of small spherulites (granular structure) appeared within the outline of the original spherulite, as seen in Figure 4b. Such granular structures have been observed before in many polymers.[2,8,25,26] These small spherulites could be caused by insufficient melting of crystal structure in the original spherulite. These surviving crystal structures will induce nucleation sites as a self-seeding effect upon subsequent crystallization. The self-seeding effect caused by insufficient melting of crystals is widely known and is often called a memory effect. The number of sites induced by self-nucleation is strongly dependent on the previous temperature of melting, its duration, and the size of the original spherulite. It is interesting to point out that the nucleation density seems to be somewhat higher at the boundary of the original spherulite than in the interior of the original spherulite. There are likely several causes for the above phenomenon, such as concentration of impurities and/or molecular fractionation at the boundary layer during crystallization. In addition to those effects, there also might be thermal history that affects at the boundary layer during reheating and crystallization. However, when the sample was completely crystallized, the nucleation density was nearly homogeneously distributed. About 90% of the melt regions remained until the number of nuclei reached saturation. These results indicate that it is unnecessary to take the migration of impurities into account. It can also be expected that the nucleation rate is higher at the center than at the boundary of the original spherulite, since the rate increases with an increase in molecular weight.[24] Therefore, the result in Figure 4 is not due to molecular fractionation. When the crystallization temperature is jumped to 180 °C from 190 °C for i-PS, lots of small spherulites appear at the boundary in a concentric structure.[8] These results indicate that the thermal history at the boundary will affect the nucleation in the subsequent remelting and crystallization. The thermal history can induce the lamella thickening at the boundary layer, which enhances the memory effect in the original spherulite. However, the reasons for the concentric structure are not clear in detail.

Figure 5 shows the relationship between the original spherulite size and the number of small spherulites (additional induced nucleation sites) within the original spherulite domain. The number of additional nucleation sites increases with an increase in the original spherulite size, and the increment of nucleation sites (slope) decreases with an increase in the melt temperature (T_f). A critical original spherulite size (R_N*) in which the new induced nucleation sites began to appear was found. The critical size of the original spherulite increases with increasing melt temperature, as shown in the inset of Figure 5. The critical size can be estimated from the spherulite growth rate (G), the induction time (τ_0), and the transition time (t_0) at which the

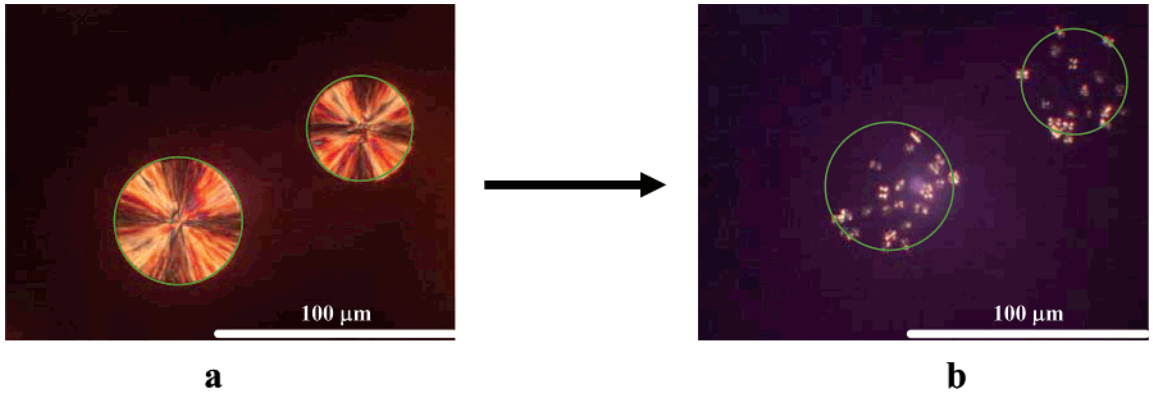

Figure 4. Optical micrographs of spherulites crystallized at 160 °C for type B: partial crystallization as a function of spherulite size, from the melt at 250 °C (T_{f1}) for a period of time (t_{c1}) exceeding the critical spherulite size (a). The sample was subsequently melted at 230 °C (T_{f2}) and then crystallized at the same crystallization temperature of 160 °C. Many small spherulites appeared within the outline of the original spherulites (b).

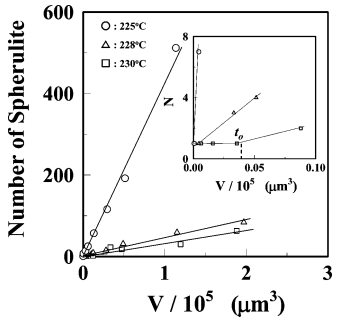

Figure 5. Plots of the number of nuclei (type B) as a function of volume of the original spherulite crystallized from the melt at three different temperatures (T_f) as indicated in the figure. The inset is for the early stages of nucleation, and t_0 denotes transition time at which additional nuclei begin to appear in the original spherulites.

Table 1. Critical Spherulite Radius (μm)[a]

T_f (°C)	R^*_N	R^*_G	R^*_S
225	2.6	2.4	1.9
228	4.8	4.8	5.8
230	9.5	9.6	7.1

[a] R^*_N is estimated from the crossover point in Figure 5, R^*_G is calculated from the spherulite growth rate (G), induction time (τ_0), and transition time (t_0) from monospherulite to granular spherulite ($R^*_G = G(t_0 - \tau_0)$), and R^*_S is estimated from the slope in Figure 5.

additional nuclei begin to appear in the original spherulites. The transition time increased with increasing melt temperature as shown in the inset of Figure 5. Values for G, τ_0, and t_0 can be obtained from the crystallization process. Thus, the calculated R_G^* ($= G(t_0 - \tau_0)$) is consistent with the critical spherulite size (R_N^*) listed in Table 1. The mean distance (R_S^*) between nucleation sites within the outline of spherulites can be estimated from the slope in Figure 5. It is interested to note that the distance between the nucleation sites coincides with the diameter of the critical spherulite listed in Table 1. A similar crystallinity effect has been found for nylon-6: the nucleation mechanism changes from sporadic nucleation to instantaneous nucleation at about 15% degree of crystallinity. The overall crystallization rate increases with a rise in the initial degree of crystallinity.[16]

The original spherulites were grown at 160 °C from the melt (T_f) until they impinged upon each other in order to completely crystallize. The completely crystallized sample was melted at 230 °C (T_{f2}) and then crystallized again at 160 °C. Here, the completely crystallized sample prepared under these conditions is defined as type C: full crystallization. The measured saturated nucleation density (N_s) for type C is plotted as a function of melt temperature (T_f) as shown in Figure 6 together with the

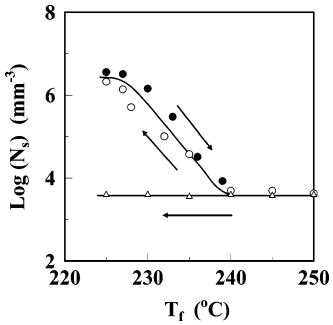

Figure 6. Relationship between saturated density of nuclei (N_s) and melt temperature (T_f) for type A: partial crystallization below the critical size (triangle) and type C: full crystallization (circle) samples. Samples were crystallized at 160 °C changing the melt temperature (T_f) from higher to lower (open circle) and from lower to higher (solid circle).

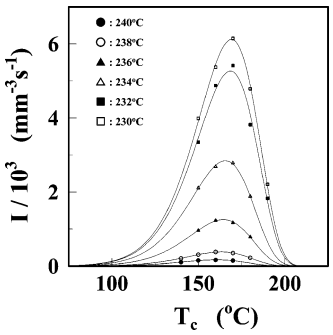

Figure 7. Crystallization temperature (T_c) dependence of nucleation rate (I) for type C crystallized from the melt at various temperatures (T_f) as indicated in the figure. Solid lines represent the best curve fitting based on eq 1. The Arrhenius expression was used for the molecular transport term.

saturation density for type A. The saturation density for type C increases by a factor of several thousand with a decrease in the melt temperature from 250 to 225 °C, whereas the saturation density for type A is a constant value. When the melt temperature was increased from 225 to 250 °C, nearly identical results were observed, as shown in Figure 6. The change in saturation density from type A to type C strongly depended on the original spherulite size as in the case of type B. A larger spherulite size resulted in a larger value for the saturated nucleus number until the original spherulites were impinged upon each other. The additional sites are caused by insufficient melting of the original spherulite. Details about the nucleation sites in the melt will be discussed in a later section.

Figure 7 shows the temperature dependence on nucleation rate as a function of the melt temperature for type C. The

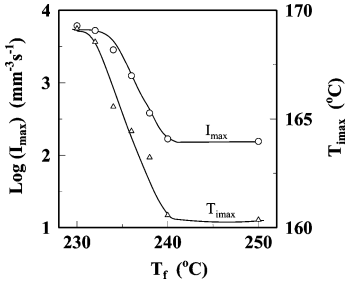

Figure 8. Plots of the maximum nucleation rate (I_{max}) (circle) and its temperature of (T_{imax}) (triangle) against the melt temperature (T_f) for type C.

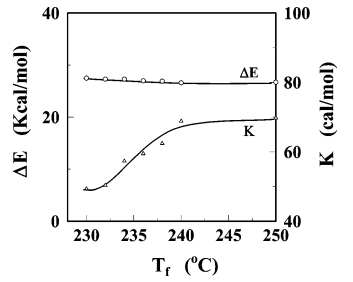

Figure 9. Plots of the activation energy of the molecular transport (ΔE) (circle) and the nucleation factor (K) (triangle) as a function of the melt temperature (T_f) for type C.

nucleation rate has a bell-shaped curve for each melt temperature and increases with decreasing melt temperature. Solid lines in Figure 7 are the results for curve fitting based on eq 1. The maximum nucleation rate (I_{max}) and temperature (T_{imax}) are plotted against the melt temperature (T_f), as shown in Figure 8. Both I_{max} and T_{imax} decrease with increasing T_f up to about 240 °C and then become constant. T_{imax} is a function of the ratio of ΔE and K.[27] Figure 9 shows the melt temperature dependence of ΔE and K estimated by curve fitting based on eq 1. Activation energy (ΔE) required for molecular transportation is nearly independent of the melt temperature. On the other hand, the factor for primary nucleation energy (K) increases with increasing melt temperature. These results indicate that the nucleation sites are induced by traces of the crystal structure in the melt as a self-seeding effect. Here, it can be assumed that the crystalline structures are not completely destroyed after melting the spherulites, and they still retain some order from the crystalline states (clusters/embryos in an amorphous state but not in a solid state) in the melt. On the basis of this type of remnant from the crystal structure, the nucleation energy was estimated from eq 1. When a primary nucleation is carried out coherently on traces of crystal structure, it can be assumed that the free surface energy on the lateral surface (σ_s) will be changed, whereas the surface free energy for the chain-folding plane (σ_e) will not be changed. Thus, the estimated ratio for the lateral surface free energy between the nucleation from the melt at 230 °C and that at 250 °C ($\sigma_{s(230\ °C)}/\sigma_{s(250\ °C)}$) is 0.84. In other words, the estimated lateral surface free energy (σ_s) for the nucleation from the melt at 230 °C decreased about 16% from that at 250 °C. Increasing the surface free energy (increasing in K) reduces the maximum crystallization temperature (T_{imax}). The small value of σ_s indicates that the order within the clusters and the amount of ordered clusters increased with decreasing melt temperature. Figure 10 shows the maximum nucleation rate (I_{max}) and the preeexponential factor of I_0 in eq 1 as a function of the saturation density (N_s). I_{max} and I_0 show a similar dependence on N_s. In fact, there is close relationship between I_{max} and I_0.[27] The ratio of I_0/I_{max} shows no molecular weight dependence.[24] I_0 and I_{max} are a function of the number

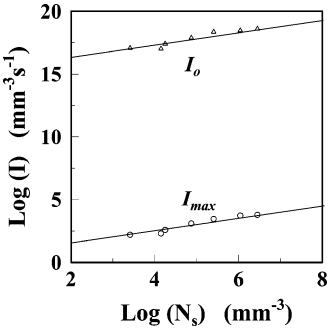

Figure 10. Plots of the maximum nucleation rate (I_{max}) (circle) and the preexponential factor (I_0) (triangle) in eq 1 against the saturated nucleation density (N_s) for type C.

of nucleation sites and can be expressed by a power law of the saturation density $N_s^{0.5}$. It is not possible at this stage to speculate on the nature of the power of 0.5.

The nucleation behavior discussed above gives a sigmoidal curve with a sporadic appearance of nuclei and a limiting number of nuclei. Such limited nucleation sites originate from insufficient melting of the original crystal structure, yielding induced nucleation sites as a self-seeding effect upon the subsequent crystallization. The self-seeding nucleation must be related to the distribution of the cluster sizes or embryos,[10,28] which are built up with crystal fragments from the insufficient melting of crystals. The cluster distribution could be associated with the saturated nucleation density (N_s). On the basis of the 90% noncrystallized area, the cluster distribution might be related to a density fluctuation based on a nucleation exclusion zone.[29] When exclusion zones overlap on the whole substrate surface, the nucleation will stop and reach saturation density. The zone might be associated with a density (or energy) fluctuation at the active nucleation sites or a density fluctuation of polymer molecules caused by diffusion and conformational changes in the molten state. The active sites could be stable at each T_f, but the number of the active sites is strongly dependent on T_f. In other words, the T_f dependence on N_s indicates the size/energy distribution of the actives sites in the melt. These active sites require an induction time (τ_0) to form the critical nucleus size followed by sporadic appearance of the nuclei.

Temperature Dependence of Helix Content. In order to investigate the cluster structure in the molten state caused by insufficient melting of spherulite structures, temperature-dependent infrared spectroscopy was used to investigate type C crystallization at 160 °C. In the infrared absorption spectrum for i-PS, there are several characteristic absorption bands[30] for 3_1-helix conformations in the polymer chain, such as 3_1 helices composed of 5 monomeric units (5-helix) at 1083 cm^{-1} and 10 monomeric units (10-helix) at 1052 cm^{-1}. In addition to these helix bands, a characteristic absorption band at 981 cm^{-1} is proportional to the degree of crystallinity (X_c).[31] The absorption band at 1026 cm^{-1} is used as an internal standard intensity band and is the characteristic band for a benzene ring in the polymer chain. Each absorption band was normalized by the peak height of the characteristic absorption band at 1026 cm^{-1}. These spectra were measured in situ at temperature intervals of 5 °C at a heating rate of 2 °C/min. Figure 11 shows the IR spectra measured at the indicated temperatures. Figure 12 shows the temperature dependence of the 5-helix, 10-helix, and X_c-normalized bands. In each of the characteristic bands, a small peak is observed at about 190 °C, and the band intensity decreases at temperatures above 204 °C. The characteristic bands for the 10-helix and the degree of crystallinity are constant at about 228 °C. However, the characteristic band of the 5-helix

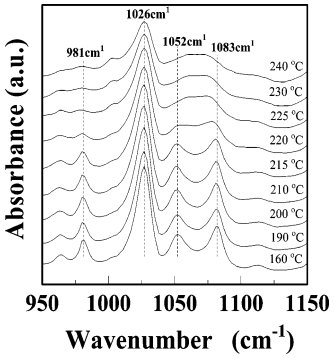

Figure 11. IR spectra for i-PS measured at the indicated temperatures during the heating process. Prior to measuring the sample was crystallized at 160 °C for 8 h.

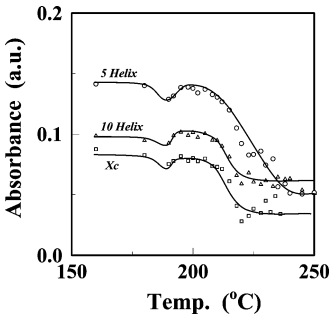

Figure 12. Change in i-PS peak intensities at 981 cm^{-1} (X_c), 1052 cm^{-1} (10-helix), and 1083 cm^{-1} (5-helix) as a function temperature during the heating process.

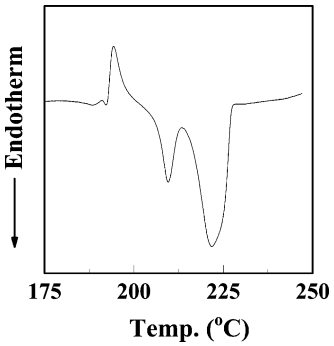

Figure 13. DSC thermogram of i-PS crystallized at 160 °C for 8 h from the melt at 250 °C.

decreases in intensity as temperature increases, becoming constant at about 240 °C. Figure 13 shows the DSC thermogram for the sample crystallized at 160 °C. An exothermic peak is observed at about 194 °C, and this peak is caused by recrystallization of the sample during heating process. Two melting endotherms are observed in the temperature range of 204−228 °C. The lower melting point increased linearly with the crystallization temperature, and its slope (the Hoffman−Weeks plot[32]) was almost 0.5, yielding an equilibrium melting temperature of 242 °C, whereas the higher melting point was nearly independent of the crystallization temperature. The higher melting peak can be explained by melting of lamellae rearranged (thickening) during the DSC heating process.[33] Comparing the results of Figures 12 and 13, the peak at 190 °C in Figure 12 can be attributed to recrystallization during heating process. The decreasing IR intensity above 204 °C can be associated with the melting of both the original and rearranged lamellae. Tails at 228 °C in the IR intensities at 1052 and 981 cm^{-1} coincide with the end of the DSC melting curve. The plot of 10-helix against X_c showed a good linear relationship. On the other hand,

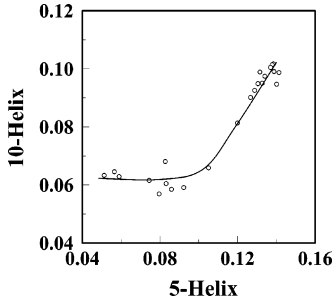

Figure 14. Plot of the peak intensity at 1052 cm^{-1} (10-helix) against the peak intensity at 1083 cm^{-1} (5-helix).

the IR band at 1083 cm^{-1} for 5-helix becomes constant at about 240 °C, which is higher than the end of the DSC melting curve. Figure 14 shows plots of the 10-helix as a function of the 5-helix, fit with two straight lines. The intersection of these two lines is consistent with the end of the melting peak. That is, the 3_1-helix composed of 5 monomeric units still remains even above the melting point and can give rise to cluster formation in the melt.

There are several publications about the temperature dependence of these helices measured by IR.[34−37] For example, Kimura et al. have reported that the peak heights of 3_1-helix bands increase sigmoidally as a function of crystallization time for i-PS crystallized at 200 °C from the melt.[34] They have found that the induction time (τ_{over}) in overall crystallization is about 50 min. However, τ_{over} is much longer than that of t_s, at which nucleation is observed to be saturated in this present study as shown in Figure 2. The crystallized region associated with the total amount of nuclei at the saturated state is about 10% in the whole specimen. Such small crystallinity in the early stage of the nucleation will be difficult to detect by usual methods such as dilatometry, DSC, X-ray, and other methods. However, the number of nuclei are much easier to observe using OM. The early stage of the crystallization process in i-PS has been also reported by Matsuba et al.[35] Their data show annealing time dependence of the 3_1-helix bands on the crystallization process at 135 °C from the glassy state. They have reported that intensities for the helix bands increase sharply in the early stage of crystallization (within 180 s) and then increase gradually. They have assumed that the gradual increase in the IR intensities continuing up to 70 min is associated with the induction period of the crystallization and that after 70 min the crystal growth is the majority contributor in IR intensities. A similar result for the induction time (about 60 min) has been found in i-PS crystallized at 130 °C from the glassy state.[37] The main increase in IR intensity beyond 180 s is related to the crystallization governed by the crystal growth rate. In fact, while the helix bands at 1052 and 1083 cm^{-1} are clearly distinguishable, the crystallinity band at 981 cm^{-1} is less evident during the induction time of the overall crystallization.[35,37] These discussions give rise to a misunderstating in the time dependence of the IR intensity, since the primary nucleation is finished before the large increase in helix bands in the overall crystallization. Here, it was noticed that for i-PS the time of t_s as indicated in Figure 2 is much shorter than induction time (τ_{over}) in the overall crystallization, which are generally measured by dilatometry, DSC, X-ray, and other methods. The induction time (τ_{over}) depends strongly on the amount of crystallized moiety, which is a function of primary nucleation rate and linear crystal growth rate. In other words, the induction time (τ_{over}) in overall crystallization is different from the induction time (τ_0) in primary nucleation.

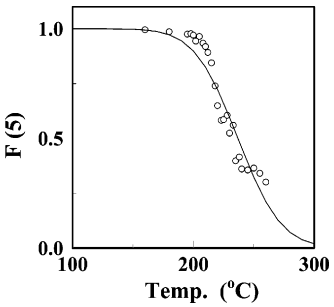

Figure 15. Temperature dependence of the peak intensity at 1083 cm^{-1} (5-helix) normalized to the intensity at 160 °C. Solid line represents curve fitting based on eq 2.

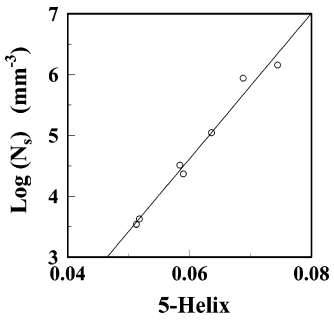

Figure 16. Relationship between the saturated nucleation density (N_s) and the amount of 3_1 helix composed of 5 monomeric units.

The temperature dependence of the 3_1-helix was analyzed theoretically by Kobayashi et al.[30] The total fraction of helices $F(m)$ composed with m monomeric units can be represented on the basis of the following simple statistical mechanical model given by eq 2.

$$F(m) = p^{m-1}[m - (m - 1)p] \tag{2}$$

where

$$p = 1/(1 + \exp[-(\Delta H - T\Delta S)/RT]) \tag{3}$$

Here, ΔH and ΔS are the enthalpy and the entropy differences per mole of monomeric units, respectively, between the random and the helical states. According to their method, the amount of the 3_1-helix composed of 5 monomeric units is plotted as a function of temperature as shown in Figure 15 (data are normalized to 160 °C). The solid curve is estimated by the best fitting procedure based on eq 2, yielding $\Delta H = 18$ kcal/mol and $\Delta S = 34$ eu/mol. These two estimated energies are larger than those reported by Kobayashi et al. Their reported values for these two energies are $\Delta H = 3.1$ kcal/mol and $\Delta S = 9.9$ eu/mol based on the 10-helix measured in a CS_2 solution from −100 °C to room temperature. The difference between the present results and those by Kobayashi et al. could result from the different states of the samples, i.e., the solution state at low temperatures vs the molten state at high temperatures. However, the activation energy for the molten state can be compared with the activation energy for the destruction of a predetermined nuclei (21.3 kcal/mol) of isotactic poly(propylene).[10] A pseudo-crystalline order can exist in the melt for a long time.[6,8,10] It is evident that a stable helix conformation exists even in a solution state,[30] in the molten state,[34] or in a glassy state.[35,37] When a crystalline sample of i-PS is melted, the longer helices in the crystal will be destroyed, but the shorter helices will be able to survive and form a cluster in the melt. Such a cluster can initiate a primary nucleation site in the melt, and its size is strongly dependent on the melt temperature. The temperature dependence of the absorption intensity of 5-helix seems to be similar the saturated nucleation density (N_s), as seen in Figure 6. Therefore, log of N_s is plotted against the 5-helix, yielding a good relationship as shown in Figure 16. This relationship indicates that the saturated nucleation density is a function of the amount of 5-helix remaining in the melt. The structure of the 5-helix might be described as irregular helices without regular packing. However, the helices are distributed randomly in length and distance among their segments. The nearest-neighbor segments to the cluster will give rise to primary nucleation sites in the melt.

Conclusions

Primary nucleation behavior of isotactic poly(styrene) was studied in a wide range of crystallization temperatures (T_c), times, and melt temperatures (T_f). Samples were melted at several melt temperatures (T_f) from 225 to 250 °C (or vice versa) and then isothermally crystallized. The time dependence on the nucleation behavior showed a sigmoidal curve with an induction time (τ_0). The spherulites sporadically appeared (the steady state of nucleation, I) until they reached a limiting number of nuclei (the saturated nucleation density, N_s). The rate of I was proportional to inverse of the induction time ($1/\tau_0$), and the product of I and τ_0 was proportional to N_s. The number of nuclei reached saturation much earlier than the induction time (τ_{over}) in the overall crystallization. N_s was not associated with impingement of spherulites, since about 90% of the melt region remained. It was found that there was a critical spherulite size, in which induced nucleation sites began to appear within the outline of the original spherulite in the subsequent crystallization. When the crystallization was stopped before reaching the critical spherulite size, there was no melt temperature dependence on the nucleation behavior. On the other hand, when spherulites were grown beyond the critical spherulite size, a large number of small spherulites (granular structure) appeared within the outline of the original spherulite in the subsequent crystallization. The number of the additional nucleation sites increased with increasing original spherulite size, and the increment of nucleation sites decreased with an increase in T_f. These granular structures could be due to insufficient melting of the crystal structure in the original spherulite, which will induce nucleation sites as a self-seeding effect upon subsequent crystallization. N_s increased by a factor of several thousand with a decrease in T_f from 250 to 225 °C. The crystallization temperature dependence on the nucleation rate has a bell-shaped curve with a maximum nucleation rate (I_{max} at T_{imax}). Both I_{max} and T_{imax} decreased with an increase in T_f up to about 240 °C and then remained constant. I_{max} is a function of the nucleation sites and is expressed by a power law of $N_s^{0.5}$. The estimated lateral surface free energy (σ_s) of the nucleation from the melt at 230 °C was about 16% lower than that at 250 °C. The nucleation density was found to be a function of the amount of 3_1-helix composed with 5 monomeric units remaining in the melt.

References and Notes

(1) Banks, W.; Sharples, A. *Makromol. Chem.* **1963**, *67*, 42.
(2) Vidotto, P. G.; Levy, D.; Kovacs, A. J. *Kolloid Z. Z. Polym.* **1969**, *230*, 289.
(3) Fillon, B.; Wittmann, J. C.; Lotz, B.; Thierry, A. *J. Polym. Sci., Polym. Phys.* **1993**, *31*, 1383.
(4) Supaphol, P.; Lin, J. S. *Polymer* **2001**, *42*, 9617.
(5) Boon, J.; Challa, G.; van Krevelen, D. W. *J. Polym. Sci., Part A2* **1968**, *6*, 1835.
(6) Reinshagen, J. H.; Dunlap, R. W. *J. Appl. Polym. Sci.* **1973**, *17*, 3619.
(7) Supaphol, P.; Spruiell, J. E. *J. Appl. Polym. Sci.* **2000**, *75*, 337.

(8) Hashimoto, M.; Amasaki, T.; Oishi, J.; Itoh, T. *Rep. Prog. Polym. Phys. Jpn.* **2000**, *43*, 739.
(9) Sisti, L.; Finell, L.; Lotti, N.; Berti, C.; Munari, A. *e-Polym.* **2003**, *54*, 1.
(10) Alfonso, G. C.; Ziabicki, A. *Colloid Polym. Sci.* **1995**, *273*, 317.
(11) Alfonso, G. C.; Scardigli, P. *Macromol. Symp.* **1997**, *118*, 323.
(12) Buerger, D. E.; Engberg, K.; Jansson, J. F.; Gedde, U. W. *Polym. Bull. (Berlin)* **1989**, *22*, 593.
(13) Khanna, Y. P.; Reimschuessel, A. C. *J. Appl. Polym. Sci.* **1988**, *35*, 2259.
(14) Moser, K.; Ohm, H.; Zwilling, W. *J. Appl. Polym. Sci.* **1991**, *48*, 459.
(15) Ziabicki, A.; Alfonso, G. C. *Macromol. Symp.* **2002**, *185*, 211.
(16) Turska, E.; Gogolewski, S. *J. Appl. Polym. Sci.* **1975**, *19*, 637.
(17) Mamun, A.; Umemoto, S.; Okui, N. *Polymer* **2006**, *47*, 5531.
(18) Sharples, A. *Polymer* **1962**, *3*, 250.
(19) Banks, W.; Hay, J. N.; Sharples, A.; Thomson, G. *Polymer* **1964**, *5*, 163.
(20) Kamide, K. *Kobunshi-Kagaku* **1967**, *24*, 259.
(21) Hay, J. N. *J. Polym. Sci., Part A2* **1965**, *3*, 433.
(22) Frish, H. L. *J. Chem. Phys.* **1957**, *27*, 90.
(23) Turnbull, D.; Fisher, J. C. *J. Chem. Phys.* **1949**, *17*, 71.
(24) Umemoto, S.; Hayashi, R; Kawano, R.; Kikutani, T.; Okui, N. *J. Macromol. Sci., Part B* **2003**, *42*, 421.
(25) Banks, W.; Gordon, M.; Sharples, A. *Polymer* **1963**, *4*, 289.
(26) Magill, J. H. *J. Appl. Phys.* **1964**, *35*, 3249.
(27) Okui, N. *J. Mater. Sci.* **1990**, *25*, 1623.
(28) Schultz, J. M. *J. Polym. Sci., Part A2* **1969**, *7*, 821.
(29) Markov, I. V. *Crystal Growth for Beginners*; World Scientific: London, 1995; p 130.
(30) Kobayashi, M.; Tsumura, K.; Tadokoro, H. *J. Polym. Sci., Part A2* **1968**, *6*, 1493.
(31) Xu, H.; Ince, S.; Cbe, P. *J. Polym. Sci., Part B* **2003**, *41*, 3026.
(32) Hoffman, J. D.; Weeks, J. J. *J. Res. Natl. Bur. Stand.* **1962**, *A66*, 13.
(33) Liu, T. *Eur. Polym. J.* **2003**, *39*, 1311.
(34) Kimura, T.; Ezure, H.; Tanaka, S.; Ito, E. *J. Polym. Sci., Part B* **1998**, *36*, 1227.
(35) Matsuba, G.; Kaji, K.; Nishida, K.; Kanaya, T. *Polym. J.* **1999**, *31*, 722.
(36) Duan, Y.; Zhang, J.; Shen, D.; Yam, S. *Macromolecules* **2003**, *36*, 4874.
(37) Zhang, J.; Duan, Y.; Shen, D.; Noda, I.; Ozaki, U. *Macromolecules* **2004**, *37*, 3292.

MA070963J